



Laser Ablation Molecular Isotopic Spectrometry

Richard E. Russo^{a,b,*}, Alexander A. Bol'shakov^b, Xianglei Mao^a, Christopher P. McKay^c, Dale L. Perry^a, Osman Sorkhabi^a

^a Lawrence Berkeley National Laboratory, University of California, Berkeley, CA 94720, USA

^b Applied Spectra, Inc., 46661 Fremont Boulevard, Fremont, CA 94538, USA

^c NASA-Ames Research Center, Moffett Field, CA 94035, USA

ARTICLE INFO

Article history:

Received 20 December 2010

Accepted 20 January 2011

Available online 31 January 2011

Keywords:

Optical isotopic measurements

Laser ablation plasma

Molecular emission spectra

Real-time chemical analysis

Chemical analysis

LAMIS

ABSTRACT

A new method of performing optical isotopic analysis of condensed samples in ambient air and at ambient pressure has been developed: Laser Ablation Molecular Isotopic Spectrometry (LAMIS). The technique uses radiative transitions from molecular species either directly vaporized from a sample or formed by associative mechanisms of atoms or ions in a laser ablation plume. This method is an advanced modification of a known atomic emission technique called laser-induced breakdown spectroscopy (LIBS). The new method – LAMIS – can determine not only chemical composition but also isotopic ratios of elements in the sample. Isotopic measurements are enabled by significantly larger isotopic shifts found in molecular spectra relative to atomic spectra. Analysis can be performed from a distance and in real time. No sample preparation or pre-treatment is required. Detection of the isotopes of hydrogen, boron, carbon, and oxygen are discussed to illustrate the technique.

© 2011 Elsevier B.V. All rights reserved.

1. Introduction

Isotopic analysis is essential in medicine, chemistry, materials science, radiochemistry, archeology, and nuclear non-proliferation. Isotopic data provide answers to fundamental questions related to research and development in these disciplines as well as providing important insight into more applied fields. This paper presents the concept and the first results obtained with newly developed Laser Ablation Molecular Isotopic Spectrometry (LAMIS) technology for real-time isotopic analyses of samples at ambient pressures. We have chosen diatomic molecules containing hydrogen, boron, and carbon as examples in this paper, but this approach can be easily extended to other diatomic and multi-atomic molecules. Benefits of such a laser based technique are rapid and direct chemical characterization of condensed samples without chemical dissolution procedures. The ultimate goal is to demonstrate a new technique for isotopic analysis with good discrimination, good sensitivity (down to ppm levels), with the potential for stand-off capability, and one that does not require (i) sample preparation or (ii) a vacuum environment for the sample.

Mass based isotopic measurements are well established and include IRMS [1,2], TIMS [3,4], SIMS [5], accelerator mass spectrometry

[6], GCMS [2,7], ICP-MS [8–10], and MALDI-MS [11]. High sensitivity and resolving power are characteristic of these mass spectrometric techniques but they generally tend to be laboratory-based and require complex sample preparation procedures. Laser ablation coupled with ICP-MS [9,10,12–14] or laser desorption in MALDI-MS eliminates the need for laborious sample preparation.

To some extent other elemental techniques also are useful for isotopic analysis. Examples include inductively coupled plasma – atomic emission spectrometry [15,16], atomic absorption spectrometry (AAS) including tunable laser AAS [17,18] and laser-excited atomic fluorescence [19,20]. Doppler-free and other high-resolution laser techniques have been detailed in several books [21,22]. Previously, optical spectroscopic techniques for isotopic analysis of both organic and inorganic samples were developed for determination of the light elements, such as hydrogen, boron, carbon, nitrogen, and oxygen [23–27]. These techniques were based on plasma sputtering or pyrolysis of the samples to convert them into a gaseous form, and spectroscopic analysis using radio-frequency discharges as a source of molecular emission excitation. The approach was mainly used for biochemical and agrochemical experiments with stable isotope tracers or labels.

Laser induced breakdown spectroscopy (LIBS) offers ideal characteristics for real-time elemental analysis at atmospheric pressure [28–30]. Several studies were conducted for isotopic analysis but only at reduced pressure [31–34], except for measuring the deuterium/hydrogen ratio [35]. Low pressure was necessary to minimize collisional, Stark and Doppler broadening of spectral lines; linewidths must be narrower than the isotopic shift. Broadening of spectral lines

* Corresponding author at: Lawrence Berkeley National Laboratory, University of California, Berkeley, CA 94720, USA.

E-mail address: rerusso@lbl.gov (R.E. Russo).

in laser-generated plasmas is known to be primarily determined by the Stark effect. At electron number density of $\sim 10^{17} \text{ cm}^{-3}$, atomic spectral linewidths are typically $\sim 0.01 \text{ nm}$. For example of isotope shifts, uranium ^{235}U and ^{238}U have an isotopic shift 0.025 nm in their respective ionic emission lines at 424.412 nm and 424.437 nm . For the plutonium isotopes ^{239}Pu and ^{240}Pu , the isotopic shift is 0.012 nm at its emission line of 594.522 nm .

Isotopic shifts can be orders of magnitude larger in molecular than atomic spectra [23–27,33] (Figs. 1 and 2). In Fig. 1, the left diagram shows the fine structure of the $2s2p^2 \ ^2D$ levels of ^{11}B (solid line). The dashed lines represent the ^{10}B levels. The directions of the ^{10}B energy level shifts with respect to the ^{11}B levels are from Ref [36]. In Boron, the net isotope effect of the ground state is zero and the ionization potential has the same value for the two isotopes [36]. The ^{11}B – ^{10}B isotopic shift from atomic emission lines for this transition is 0.46 cm^{-1} , or 0.002 nm , which is several orders of magnitude smaller than the isotopic shift measured for boron monoxide. The measured shift for BO is 113 cm^{-1} or 0.73 nm for the $B^2\Sigma^+ (v=0) \rightarrow X^2\Sigma^+ (v=2)$ transition.

Atomic isotope shifts depend on the transition [37]. The data in Fig. 2 represent prominent lines used in emission spectroscopy. Molecular isotope pairs (Fig. 2) used in this work are listed in Table 1. Molecular vibronic (i.e. vibrational, rotational, and electronic) emission wavelengths depend on the rotational and vibrational energy levels between two different electronic states (see Fig. 1):

$$\nu = T' - T'' = (T'_e - T''_e) + (G'_v - G''_v) + (F'_j - F''_j) \quad (1)$$

where the single primed symbols refer to the upper state and double primed symbols refer to lower state; T_e is the electronic energy, G_v is the

vibrational energy, and F_j is the rotational energy. Expressions for G and F can be found in literature [38–41]; they can be used for spectrum simulation and fitting to measured spectra, thus enabling calculation of isotope abundances. The molecular emission intensity is the function of temperature:

$$I = C_{em} \frac{q_{v'v''} S_{j'j''}}{Q_{v'}} \nu^4 e^{-E/kT} \quad (2)$$

where C_{em} is the emission coefficient, $q_{v'v''}$ is the Franck–Condon factor and $S_{j'j''}$ is the Hönl–London factor. Q is the partition function and ν is the optical emission light frequency. E is the upper energy and k is the Boltzmann constant.

The effect of mass difference between isotopes is primarily observed in terms G_v and F_j of vibronic transitions, while for the electronic component, T_e the mass effect is significantly smaller. Consequently, molecular transitions involving change of vibrational and rotational states can exhibit significantly larger isotopic shifts than atomic transitions which are purely electronic in nature (Fig. 2). Larger isotopic shifts significantly simplify measurement requirements. Isotope ratio measurements from molecular spectra are advantageous for light elements (Fig. 2) that are particularly important for biological organic life sciences. For heavy elements, the molecular isotopic effect is smaller because it scales with the reduced mass of the formed molecules. Moreover, the vibrational and rotational lines in heavy molecules are closer than in light molecules.

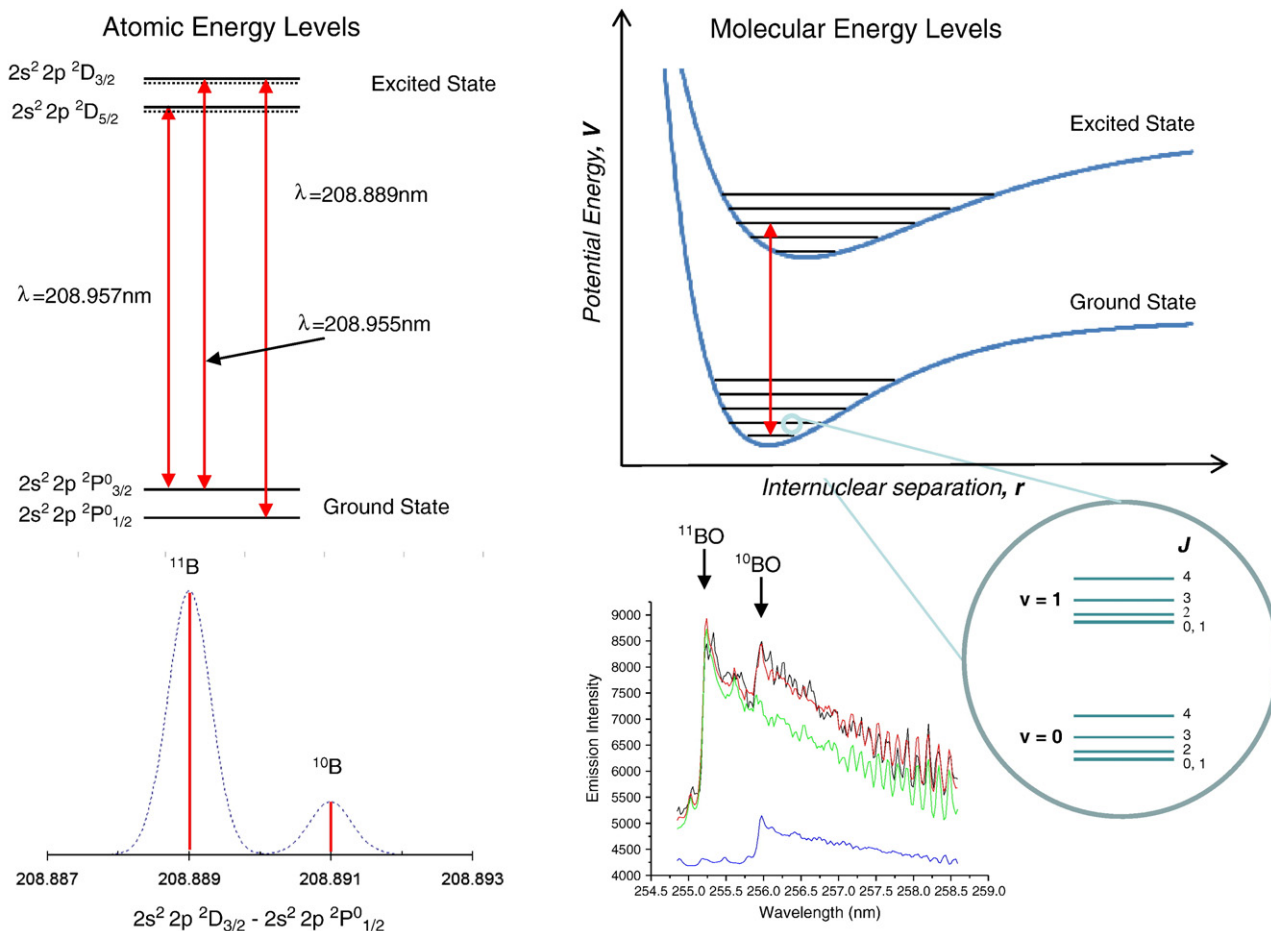


Fig. 1. Energy diagram of $2s^2 2p^2 \ ^2P_{1/2, 3/2} \leftarrow 2s^2 2p^2 \ ^2D_{5/2, 3/2}$ electronic transitions of atomic boron is shown on the left (not to scale). The measured ^{11}B and ^{10}B isotopic shift for this transition is 0.46 cm^{-1} or 0.002 nm . The measured shift for the BO transition $B^2\Sigma^+ (v=0) \rightarrow X^2\Sigma^+ (v=2)$ is 113 cm^{-1} or 0.73 nm .

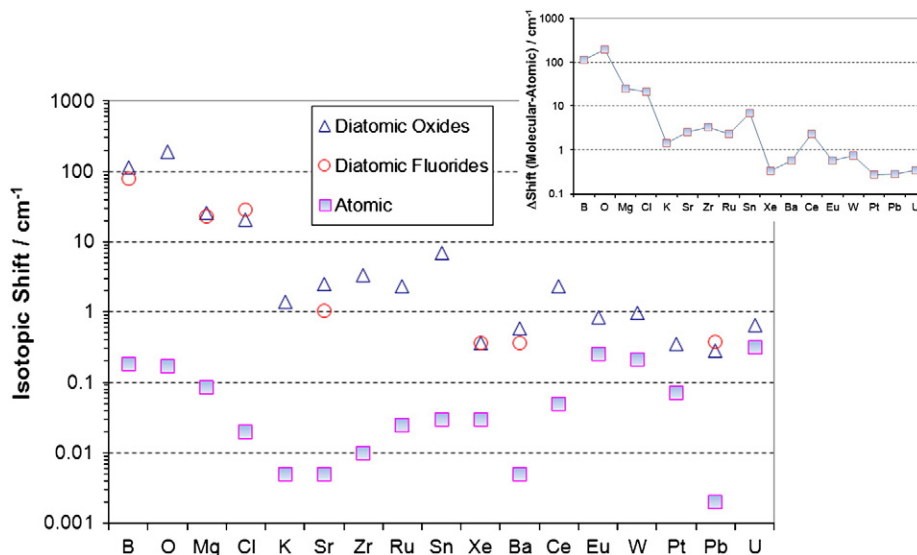


Fig. 2. Molecular vs. atomic isotopic shifts for various elements. Molecular shifts were calculated for either the diatomic oxide or fluoride for each element considered in this plot. Isotopic shifts are much larger, up to several orders of magnitude, for molecular species as opposed to atomic species. The inset is a difference plot of isotopic shifts. Atomic isotopic shift values were taken from Stern and Snively [37].

2. Demonstration of the new concept

This paper presents the concept and the first results obtained with newly developed Laser Ablation Molecular Isotopic Spectrometry (LAMIS) technology for real-time isotopic analyses of samples at ambient pressure. Sample ablation for the experiments reported here was achieved by using a Nd:YAG laser operating at 1064 nm with a typical pulse energy of 50 mJ and a pulse width of 4 ns. The laser beam was focused onto the sample with a quartz lens to a spot diameter of $\sim 100 \mu\text{m}$ in ambient air. A second lens was used to collect the laser-induced plasma emission onto the entrance of a fiber optic cable coupled to a Czerny–Turner spectrometer. At a specific time delay after the laser pulse, the dispersed emission was recorded by an Intensified Charge-Coupled Device (ICCD). The delay was optimized to detect molecular emission, while minimizing atomic and continuum intensities. The measured spectra were averaged over several laser shots (listed in figure captions).

Isotopic shifts in the measured molecular spectra can be observed in both vibrational and rotational molecular band structures. Fig. 3 shows the vibrational band head positions of $^{10}\text{B}^{16}\text{O}$ and $^{11}\text{B}^{16}\text{O}$ and demonstrates the large molecular isotopic shift. The blue and green

curves represent the calculated emission spectra for $^{10}\text{B}^{16}\text{O}$ and $^{11}\text{B}^{16}\text{O}$, respectively. The isotopic shift for this band is 0.73 nm. By contrast, the isotopic shift of atomic boron at 208.889 nm is orders of magnitude smaller at 0.0025 nm.

For isotopic detection, we can use the spectral shifts of vibrational band head or the rotational line positions. For vibrational band head differences, isotopic shift can be expressed as:

$$\Delta\nu = (1-\rho) \left[\omega_e' \left(v' + \frac{1}{2} \right) - \omega_e'' \left(v'' + \frac{1}{2} \right) \right] - (1-\rho^2) \left[\omega_e' x_e' \left(v' + \frac{1}{2} \right)^2 - \omega_e'' x_e'' \left(v'' + \frac{1}{2} \right)^2 \right] \quad (3)$$

where $\rho = \sqrt{\mu/\mu_i}$, μ is the reduced mass of the molecule, and i denotes the isotope [38]. According to Eq. (3), the isotopic shift is large if the difference between vibrational quantum numbers $\Delta\nu$ is also

Table 1
Molecular isotope shifts calculated using molecular constants.

Element	Isotope pair	Vibration band	Diatomic oxide shift (cm^{-1})	Diatomic fluoride shift (cm^{-1})
Boron	^{10}B , ^{11}B	(0–2)	113.505	79.344
Oxygen	^{16}O , ^{18}O	(0–2)	193.480	
Magnesium	^{24}Mg , ^{26}Mg	(1–0)	25.382	22.861
Chlorine	^{35}Cl , ^{37}Cl	(0–2)	21.013	29.030
Potassium	^{39}K , ^{41}K	(0–1)	1.413	
Strontium	^{86}Sr , ^{88}Sr	(0–1)	2.520	1.050
Zirconium	^{90}Zr , ^{94}Zr	(0–1)	3.291	
Ruthenium	^{102}Ru , ^{104}Ru	(0–1)	2.300	
Tin	^{116}Sn , ^{120}Sn	(0–2)	7.004	
Xenon	^{129}Xe , ^{132}Xe	(0–1)		0.362
Barium	^{137}Ba , ^{138}Ba	(0–1)	0.588	0.363
Cerium	^{140}Ce , ^{142}Ce	(0–1)	2.367	
Europium	^{151}Eu , ^{153}Eu	(1–0)	0.834	
Tungsten	^{182}W , ^{184}W	(0–1)	0.959	
Platinum	^{194}Pt , ^{195}Pt	(0–1)	0.346	
Lead	^{206}Pb , ^{208}Pb	(0–1)	0.285	0.380
Uranium	^{235}U , ^{238}U	(1–0)	0.657	

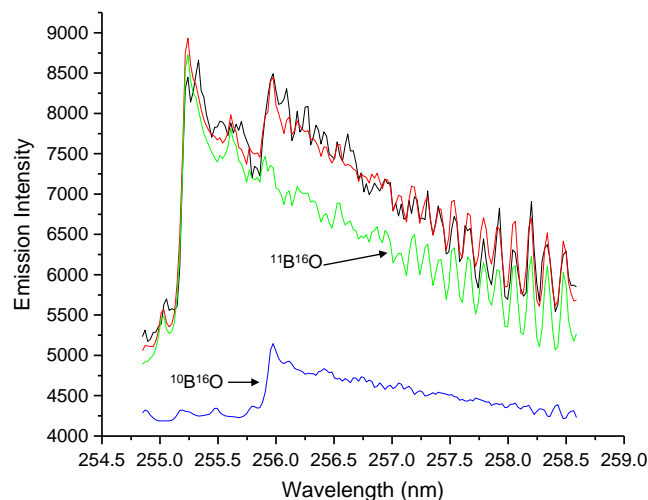


Fig. 3. Experimental and calculated emission spectra for boron monoxide, BO. The black curve represents the measured spectrum with natural isotopic abundance of boron accumulated from 100 laser pulses, while the red curve represents the fitted spectrum with 20.24% of $^{10}\text{B}^{16}\text{O}$. The blue and green curves represent the calculated emission spectra of the $^{10}\text{B}^{16}\text{O}$ and $^{11}\text{B}^{16}\text{O}$, respectively.

large. When choosing vibrational band heads for isotopic detection, transitions with the largest $\Delta\nu$ and reasonable emission intensities should be used.

The emission spectra in Fig. 3 represent transitions of the (0, 2) band of the $X^2\Sigma^+ - B^2\Sigma^+$ system for boron monoxide. These data were measured from the plasma plume of a laser ablated solid pellet of boron nitride in air and at atmospheric pressure. The black line plot is the experimental spectrum of BO with the ^{11}B and ^{10}B ratio being the naturally occurring isotopic abundance of 80.2% and 19.8%, respectively. The other plots are calculated spectra using Eqs. (1) and (2). The results in Fig. 3 can be used to determine the isotopic concentration and demonstrate the isotopic detection capabilities of using molecular emission. Using a least squares fitting technique, the experimental data were fit by varying the isotopic fraction. The fit resulted in a calculated concentration of 20.2% for ^{10}B , which is very close to the natural abundance of 19.8% for ^{10}B .

Rotational structure also can be used for isotopic detection. The isotopic shift for rotational energy in diatomic molecules is:

$$\Delta F = (1 - \rho^2) [B'_v J'(J' + 1) - B''_v J''(J'' + 1)] \quad (4)$$

According to Eq. (4), the isotopic shift depends on both vibrational and rotational quantum numbers and increases with both J and v . As an example, the wide range of boron monoxide rotational structure between 350 and 700 nm represent vibronic transitions of the BO $A^2\Pi_i - X^2\Sigma^+$ system. Fig. 4 shows a narrow spectral range of this system for enriched and naturally occurring boron monoxide which resulted from the laser ablation of the following samples: $^{10}\text{B}_2\text{O}_3$ (99% ^{10}B , red curve), $^{11}\text{B}_2\text{O}_3$ (95% ^{11}B , green curve), and boron nitride (80.2% ^{11}B and 19.8% ^{10}B , the naturally occurring abundance for boron, black curve). Some of the lines observed in the spectrum of the mixture of the two isotopes are attributed to ^{10}B , while others belong to ^{11}B . The strong line at 583.75 nm is indicative of ^{10}B from the BO radical formed at the highest plasma temperature. As an example, this peak may be used to identify ^{10}B in a mixture of the two boron isotopes and to quantify isotopic concentration of ^{10}B in the sample.

The concentration of individual isotopes also can be determined using Partial Least-Squares (PLS) calibration procedure. The PLS

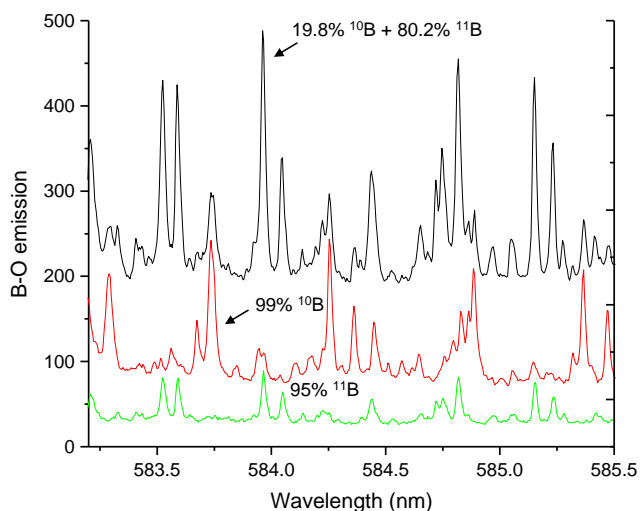


Fig. 4. Boron monoxide rotational band spectra obtained from ablation of $^{10}\text{B}_2\text{O}_3$, $^{11}\text{B}_2\text{O}_3$, and BN. The isotopic ratio of boron is the natural isotopic abundance for BN. The black curve represents boron oxide ro-vibronic emission with the natural isotope abundance. The red and green curves represent the rotational-emission of the $^{10}\text{B}^{16}\text{O}$ and $^{11}\text{B}^{16}\text{O}$, respectively. The spectra from BN accumulated using 30 laser pulses and spectra from B_2O_3 accumulated using 60 laser pulses.

model for boron isotopes was established using ten LAMIS reference spectra. Each spectrum was accumulated from six laser pulses from $^{10}\text{B}_2^{16}\text{O}_3$ (99% ^{10}B) and $^{11}\text{B}_2^{16}\text{O}_3$ (95% ^{11}B) samples. Boron nitride with natural abundance was used as the unknown sample. Three laser pulses were accumulated for each spectra and ten of these spectra were measured. The ^{11}B concentration was calculated to be $80.5 \pm 0.9\%$. With this PLS calibration model, an estimated detection limit for ^{10}B isotope was approximately 1% in boron nitride.

In another experiment, vapors of ordinary water (H_2O) and heavy water (D_2O) were ablated; the OH and OD molecular emission from the plasma plume was measured. Molecular spectra in a laser-generated plasma become relatively stronger at longer time delays. The gate width of the ICCD detector was set to 60 μs with the delay of 25 μs , contrary to a usual value of $\sim 1 \mu\text{s}$ typically used for atomic emission detection in LIBS measurements. The data in Fig. 5 clearly demonstrate the prominent spectral features of OH $A^2\Sigma^+ - X^2\Pi_i$ (0,0) transition at $\sim 306 \text{ nm}$ (R_1, R_2 branch heads) and $\sim 309 \text{ nm}$ (Q_2 branch head) with partially resolved individual rotational lines. The experimental shift between the Q_2 branch heads of OH and OD is approximately 0.68 nm. This shift is larger than the 0.18 nm separation between H and D atomic lines at 656.29 and 656.11 nm, respectively. However, more important in this case is that the hydroxyl spectra are significantly less prone to Stark broadening than atomic lines of H and D. Spectral lines of light atoms such as hydrogen and deuterium can be broadened up to $\sim 1 \text{ nm}$ width in laser ablation plasmas. Segregation of H and D has been measured in laser induced and DC arc plasmas [34,42]. The possibility of segregation could influence these molecular spectral measurements, and needs to be investigated. However, at the long delay time and atmospheric pressure used in this work, multiple collisions between ablated and atmospheric species would likely equilibrate the spatial isotopic distribution.

Simulation of the ^{16}OH , ^{18}OH , and ^{16}OD vibronic spectra demonstrate that sufficient spectral resolution ($\sim 0.03 \text{ nm}$) to selectively detect all these species simultaneously can be attained with modern compact echelle-based spectrometers. In laser ablation, the number density of species vaporized in each laser shot is usually $10^{15} - 10^{19} \text{ cm}^{-3}$. Most of the molecular species in a plume ejected from water are expected to be ^{16}OH . Following the isotopic abundances, the number of ^{18}OH radicals will be approximately 500 times less. Therefore, the estimated ^{18}OH number density of at least $\sim 10^{12} \text{ cm}^{-3}$ in a laser-vaporized plume from water ice can be expected. Such

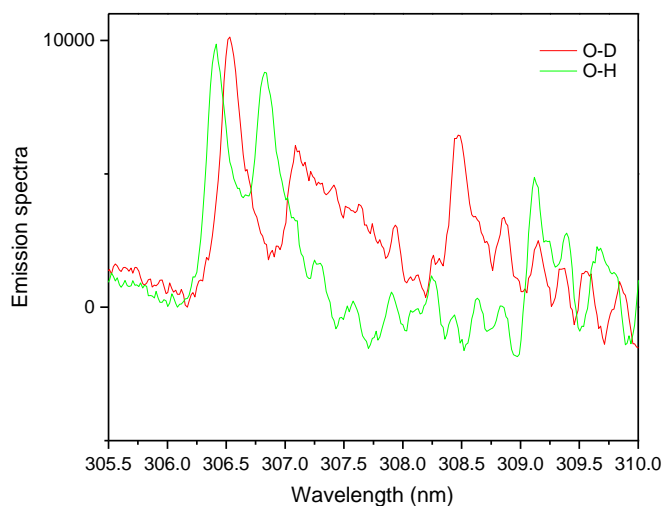


Fig. 5. Emission band of OH and OD generated from water and deuterium monoxide, respectively. The green curve represents the OH spectrum, while the red curve represent the OD spectrum. Spectra accumulated from 600 laser pulses.

quantities of species are readily detectable in emission spectroscopy. The real-time determination of oxygen isotopes from ice will be of significant consequence to studies in paleoclimatology, hydrogeology and glaciology.

Additional experiments were performed to measure carbon isotopes. LAMIS measurements of carbon isotopic signatures were accomplished using diatomic CN and C₂ radicals that are known to form effectively in laser ablation plumes and are among the well-investigated species. The experiments were performed with regular graphite (99% ¹²C) and isotopically enriched urea (99% ¹³C) as the ablation samples. The C₂ from the sample and N₂ from ambient air are the precursors for CN formation in laser ablation plasma. The CN radicals are generated in comparable abundance to C₂ and both these species are routinely observed in LIBS of carbon-containing samples. At near-threshold ablation of graphite, vapor in the plume is dominated by C₂ and C₃ radicals that are directly ejected as the intact molecules. Evaporation of carbon in the molecular versus atomic form is thermodynamically favored because of relatively high bond energies of C₂ and C₃. With the increasing laser fluence, molecular emission remains roughly constant while atomic carbon emission increases drastically indicating the major fraction of the plume becomes atomized [43].

The spectra of C₂ and CN with resolved features attributed to ¹²C and ¹³C isotopes measured in laser ablation plasmas are presented in Fig. 6. The data in Fig. 6 display the (0,0) band head regions of the C₂ d³Π_g – a³Π_u (Swan system) and CN B²Σ⁺ – X²Σ⁺ transitions, respectively. The isotopic shifts in the band heads of both radicals are similar and approximately equal to ~0.03 nm. The heavier isotope spectrum in CN is shifted toward the violet, but the counterpart in C₂ is shifted toward the red. Simulation of the C₂ spectrum in the region 875–890 nm of the Phillips band (2,0) of the electronic system A¹Π_u – X¹Σ_g⁺ indicated that the isotopic shift between ¹²C₂ and ¹²C¹³C can be as large as ~0.3 nm. A similar conclusion was drawn from the simulation of ¹²C¹⁴N and ¹³C¹⁴N spectra in the region of the A²Π_i – X²Σ⁺ (1,0) transition between 925 and 940 nm. In the latter wavelength region, the three isomeric molecules ¹²C¹⁴N, ¹³C¹⁴N, and ¹²C¹⁵N can be individually resolved with resolution of ~0.03 nm.

While the experimental results presented in this paper were obtained using optical emission measurements, other optical spectroscopic techniques, such as absorption and induced fluorescence, can be applied in a similar fashion within the LAMIS technique

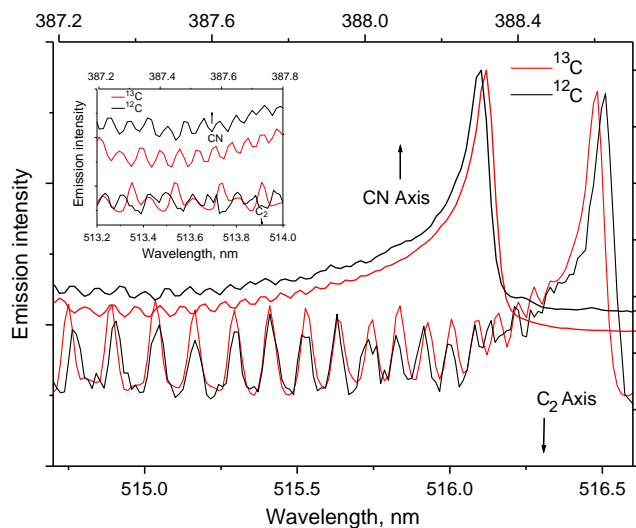


Fig. 6. Emission spectra of CN and C₂ generated from ¹³C-enriched urea and predominantly ¹²C graphite. The inset is a zoomed in region of the spectrum showing the isotopic shifts for ¹²C and ¹³C in the measured C₂ and CN spectra. Spectra accumulated from 100 laser pulses.

described in this paper. Laser induced fluorescence and advanced absorption techniques (e.g., wavelength modulation spectroscopy, cavity ringdown spectroscopy, cavity-enhanced spectroscopy, etc.) can be significantly more sensitive than emission spectroscopy. High sensitivity is important for detection of minor isotopes. On the other hand, simplicity and compactness of equipment required for the direct emission detection is a significant merit of LAMIS.

Acknowledgements

This work was supported by the Defense Threat Reduction Administration (DTRA) of the U. S. Department of Defense under federal award nos. LB09005541 and LB09005541A; and contract no. DE-AC02-05CH11231 awarded by the U.S. Department of Energy through the National Nuclear Security Administration (NNSA); and NASA contract no. NNX10CA07C awarded to Applied Spectra Inc.

References

- [1] I.T. Platzner, K. Habfast, A.J. Walder, A. Goetz, *Modern Isotope Ratio Mass Spectrometry*, Wiley, London, 1997.
- [2] A. de Korompay, J.C. Hill, J.F. Carter, N. NicDaeid, R. Sleeman, Supported liquid-liquid extraction of the active ingredient (3, 4-methylenedioxyethylamphetamine) from ecstasy tablets for isotopic analysis, *J. Chromatogr. A* 1178 (2008) 1–8.
- [3] S. Richter, S.A. Goldberg, Improved techniques for high accuracy isotope ratio measurements of nuclear materials using thermal ionization mass spectrometry, *Int. J. Mass Spectrom.* 229 (2003) 181–197.
- [4] J. Harvey, E.F. Baxter, An improved method for TIMS high precision neodymium isotope analysis of very small aliquots (1–10 ng), *Chem. Geol.* 258 (2009) 251–257.
- [5] A. Benninghoven, F.G. Rüdener, H.W. Werner, *Secondary Ion Mass Spectrometry: Basic Concepts, Instrumental Aspects, Applications, and Trends*, Wiley, New York, 1987.
- [6] C. Tuniz, R. Bird, D. Fink, G.F. Herzog, *Accelerator Mass Spectrometry: Ultra-sensitive Analysis for Global Science*, CRC Press, Boca Raton, 1998.
- [7] J.A.J. Dungait, R. Bol, I.D. Bull, R.P. Evershed, Tracking the fate of dung-derived carbohydrates in a temperate grassland soil using compound-specific stable isotope analysis, *Org. Geochem.* 40 (2009) 1210–1218.
- [8] M. Liezers, S.A. Lehn, K.B. Olsen, O.T. Farmer, D.C. Duckworth, Determination of plutonium isotope ratios at very low levels by ICP-MS using on-line electrochemically modulated separations, *J. Radioanal. Nucl. Chem.* 282 (2009) 299–304.
- [9] P.Z. Vroon, B. van der Wagt, J.M. Koornneef, G.R. Davies, Problems in obtaining precise and accurate Sr isotope analysis from geological materials using laser ablation MC-ICPMS, *Anal. Bioanal. Chem.* 390 (2008) 465–476.
- [10] A.I.S. Kemp, G.L. Foster, A. Schersten, M.J. Whitehouse, J. Darling, C. Storey, Concurrent Pb–Hf isotope analysis of zircon by laser ablation multi-collector ICP-MS, with implications for the crustal evolution of Greenland and the Himalayas, *Chem. Geol.* 261 (2009) 244–260.
- [11] MALDI MS: a practical guide to instrumentation, in: F. Hillenkamp, J. Peterkatalinic (Eds.), *Methods and Applications*, Wiley-VCH, Weinheim, 2007.
- [12] F. Poitrasson, X. Mao, S.S. Mao, R. Freyrier, R.E. Russo, Comparison of ultraviolet femtosecond and nanosecond laser ablation inductively coupled plasma mass spectrometry analysis in glass, monazite, and zircon, *Anal. Chem.* 75 (2003) 6184–6190.
- [13] J. Gonzalez, D. Oropeza, X. Mao, R.E. Russo, Assessment of the precision and accuracy of thorium (²³²Th) and uranium (²³⁸U) measured by quadrupole based inductively coupled plasma-mass spectrometry using liquid nebulization, nanosecond and femtosecond laser ablation, *J. Anal. At. Spectrom.* 23 (2008) 229–234.
- [14] R.E. Russo, X. Mao, J. Gonzalez, S.S. Mao, Femtosecond laser ablation ICP-MS, *J. Anal. At. Spectrom.* 17 (2002) 1072–1075.
- [15] M.C. Edelson, V.A. Fassel, Isotopic abundance determinations by inductively coupled plasma atomic emission spectroscopy, *Anal. Chem.* 53 (1981) 2345–2347.
- [16] D.P. Baldwin, D.S. Zamzow, A.P. D'Silva, High-resolution spectroscopy using an acousto-optic tunable filter and a fiber-optic Fabry–Perot interferometer, *Appl. Spectrosc.* 50 (1996) 498–503.
- [17] H. Liu, A. Quentmeier, K. Niemax, Diode laser absorption measurement of uranium isotope ratios in solid samples using laser ablation, *Spectrochim. Acta Part B* 57 (2002) 1611–1623.
- [18] L.A. King, I.B. Gornushkin, D. Pappas, B.W. Smith, J.D. Winefordner, Rubidium isotope measurements in solid samples by laser ablation-laser atomic absorption spectroscopy, *Spectrochim. Acta Part B* 54 (1999) 1771–1781.
- [19] B.W. Smith, A. Quentmeier, M. Bolshov, K. Niemax, Measurement of uranium isotope ratios in solid samples using laser ablation and diode laser-excited atomic fluorescence spectrometry, *Spectrochim. Acta Part B* 54 (1999) 943–958.
- [20] B.W. Smith, I.B. Gornushkin, L.A. King, J.D. Winefordner, A laser ablation-atomic fluorescence technique for isotopically selective determination of lithium in solids, *Spectrochim. Acta Part B* 53 (1998) 1131–1138.
- [21] V.S. Letokhov, V.P. Chebotayev, *Nonlinear Laser Spectroscopy*, Springer-Verlag, Berlin, 1977.

- [22] E.W. Otten, Investigation of Short-Lived Isotopes by Laser Spectroscopy, Harwood Academic Publishers, Chur, 1989.
- [23] N.A. Zakorina, G.S. Lazeeva, A.A. Petrov, Spectroscopic determination of the isotopic composition of boron trifluoride, *J. Nucl. Energy* 21 (1967) 309–313.
- [24] N.A. Zakorina, A.A. Petrov, Isotopic spectral analysis of oxygen in a hot hollow cathode, *J. Appl. Spectrosc.* 23 (1975) 1157–1160.
- [25] G.S. Lazeeva, A.A. Petrov, R.V. Khomyakov, Spectral-isotope method for determining carbon in biological objects, *J. Appl. Spectrosc.* 25 (1976) 1199–1205.
- [26] G.S. Lazeeva, V.M. Nemets, A.A. Petrov, Spectral-isotopic method of determination of gas-forming elements in organic and inorganic substances, *Spectrochim. Acta Part B* 36 (1981) 1233–1242.
- [27] V.M. Nemets, I.A. Rodushkin, A.A. Solov'ev, V.N. Funtov, Isotopic carbon analysis using the C₂ molecule spectrum, *J. Appl. Spectrosc.* 52 (1990) 461–465.
- [28] R.E. Russo, X. Mao, C. Liu, J. Gonzalez, Laser assisted plasma spectrochemistry: laser ablation, *J. Anal. Atom. Spectrom.* 19 (2004) 1084–1089.
- [29] R.E. Russo, X. Mao, S.S. Mao, The physics of laser ablation in microchemical analysis, *Anal. Chem.* 74 (2002) 70A–77A.
- [30] R.W. Bogue, Boom time for LIBS technology, *Sensor Rev.* 24 (2004) 353–357.
- [31] W. Pietsch, A. Petit, A. Briand, Isotope ratio determination of uranium by optical emission spectroscopy on a laser-produced plasma – basic investigations and analytical results, *Spectrochim. Acta Part B* 53 (1998) 751–761.
- [32] C.A. Smith, M.A. Martinez, D.K. Veirs, D.A. Cremers, Pu-239/Pu-240 isotope ratios determined using high resolution emission spectroscopy in a laser-induced plasma, *Spectrochim. Acta Part B* 57 (2002) 929–937.
- [33] H. Niki, T. Yasuda, I. Kitazima, Measurement technique of boron isotopic ratio by laser-induced breakdown spectroscopy, *J. Nucl. Sci. Technol.* 35 (1998) 34–39.
- [34] L. Mercadier, J. Hermann, C. Grisolia, A. Semerok, Plume segregation observed in hydrogen and deuterium containing plasmas produced by laser ablation of carbon fiber tiles from a fusion reactor, *Spectrochim. Acta Part B* 65 (2010) 715–720.
- [35] A. D'Ulivo, M. Onor, E. Pitzalis, R. Spiniello, L. Lampugnani, G. Cristoforetti, S. Legnaioli, V. Palleschi, A. Salvetti, E. Tognoni, Determination of the deuterium/hydrogen ratio in gas reaction products by laser-induced breakdown spectroscopy, *Spectrochim. Acta Part B* 61 (2006) 797–802.
- [36] B. Edian, A. Olme, G. Herzberg, J.W.C. Johns, Ionization potential of boron, and the isotopic and fine structure of 2s2p² ²D, *J. Opt. Soc. Am.* 60 (1970) 889.
- [37] R.C. Stern, B.B. Snavely, The Laser Isotope Separation Program at Lawrence Livermore Laboratory, *Ann. NY Acad. Sci.* 267 (1976) 71–79.
- [38] G. Herzberg, Molecular spectra and molecular structure, I, Spectra of Diatomic Molecules, 2nd Ed., Van Nostrand Reinhold, New York, 1950.
- [39] E.L. Hill, J.H. Van Vleck, On the quantum mechanics of the rotational distortion of multiplets in molecular spectra, *Phys. Rev.* 32 (1928) 250.
- [40] J.H. Van Vleck, On σ -type doubling and electron spin in the spectra of diatomic molecules, *Phys. Rev.* 33 (1929) 467–506.
- [41] J.H. Van Vleck, The coupling of angular momentum vectors in molecules, *Rev. Mod. Phys.* 23 (1951) 213–227.
- [42] D. Vukanovic, V. Vukanovic, On the behaviour of hydrogen isotopes in a d.c. arc plasma, *Spectrochim. Acta Part B* 24 (1969) 579–683.
- [43] L. St-Onge, R. Sing, S. Béchar, M. Sabsabi, Carbon emissions following 1.064 μ m laser ablation of graphite and organic samples in ambient air, *Appl. Phys. A* 69 (1999) S913–S916.